
Dossier

*This paper is a part of the hereunder thematic dossier published in OGST Journal, Vol. 70, No. 5, pp. 791-902 and available online here*

Cet article fait partie du dossier thématique ci-dessous publié dans la revue OGST, Vol. 70, n°5, pp. 791-902 et téléchargeable ici

DOSSIER Edited by/Sous la direction de : **D. Uzio**

*IFP Energies nouvelles International Conference / Les Rencontres Scientifiques d'IFP Energies nouvelles*

# *PHOTO4E – Photocatalysis for energy*

# PHOTO4E – Photocatalyse pour l'énergie

*Oil & Gas Science and Technology – Rev. IFP Energies nouvelles*, Vol. 70 (2015), No. 5, pp. 791-902




IFP Energies nouvelles

*Oil & Gas Science and Technology – Rev. IFP Energies nouvelles*, Vol. 70 (2015), No. 5, pp. 891-902

DOI: 10.2516/ogst/2014062



*IFP Energies nouvelles International Conference*
Rencontres Scientifiques d'IFP Energies nouvelles

*PHOTO4E – Photocatalysis for energy*
PHOTO4E – Photocatalyse pour l'énergie

# Simultaneous Production of $CH_4$ and $H_2$ from Photocatalytic Reforming of Glucose Aqueous Solution on Sulfated Pd-$TiO_2$ Catalysts

Vincenzo Vaiano[1], Giuseppina Iervolino[1], Giuseppe Sarno[1], Diana Sannino[1*], Luigi Rizzo[2], Julie J. Murcia Mesa[3,4], Maria C. Hidalgo[4] and Jose A. Navío[4]

[1] *Department of Industrial Engineering, University of Salerno, via Giovanni Paolo II, 132, 84084 Fisciano (SA) - Italy*
[2] *Department of Civil Engineering, University of Salerno, via Giovanni Paolo II, 132, 84084 Fisciano (SA) - Italy*
[3] *Universidad Pedagógica y Tecnológica de Colombia, Avenida Central del Norte, Tunja, Boyacá - Colombia*
[4] *Instituto de Ciencia de Materiales de Sevilla (ICMS), Consejo Superior de Investigaciones Científicas (CSIC), Universidad de Sevilla, Américo Vespucio 49, 41092 Sevilla - Spain*
*e-mail: dsannino@unisa.it*

* Corresponding author

***Abstract*** *— In this work, the simultaneous production of $CH_4$ and $H_2$ from photocatalytic reforming of glucose aqueous solution on Pd-$TiO_2$ catalysts under UV light irradiation by Light-Emitting Diodes (LED) was investigated. The Pd-$TiO_2$ catalysts were prepared by the photodeposition method. The Pd content was in the range 0.5-2 wt% and a photodeposition time in the range 15-120 min was used. Pd-$TiO_2$ powders were extensively characterized by X-Ray Diffraction (XRD), $S_{BET}$, X-Ray Fluorescence spectrometry (XRF), UV-Vis Diffuse Reflectance Spectra (UV-Vis DRS), TEM and X-Ray Photoelectron Spectroscopy (XPS). It was found that the lower Pd loading (0.5 wt%) and 120 min of photodeposition time allowed us to obtain homogeneously distributed metal nanoparticles of small size; it was also observed that the increase in the metal loading and deposition time led to increasing the $Pd^0$ species effectively deposited on the sulfated $TiO_2$ surface. Particle size and the oxidation state of the palladium were the main factors influencing the photocatalytic activity and selectivity. The presence of palladium on the sulfated titania surface enhanced the $H_2$ and $CH_4$ production. In fact, on the catalyst with 0.5 wt% Pd loading and 120 min of photodeposition time, $H_2$ production of about 26 µmol was obtained after 3 h of irradiation time, higher than that obtained with titania without Pd (about 8.5 µmol). The same result was obtained for the methane production. The initial pH of the solution strongly affected the selectivity of the system. In more acidic conditions, the production of $H_2$ was enhanced, while the $CH_4$ formation was higher under alkaline conditions.*

**Résumé — Production simultanée de $CH_4$ et $H_2$ par réformage photocatalytique d'une solution aqueuse de glucose sur un catalyseur Pd-$TiO_2$ sulfaté** — Dans cette recherche, la production simultanée de $CH_4$ et $H_2$ par le reformage photocatalytique de glucose sur les catalyseurs Pd-$TiO_2$ sous irradiation de lumière UV réalisée par des diodes électroluminescentes (LED) a été étudiée. Les échantillons de Pd-$TiO_2$ ont été préparés par la méthode de photodéposition. Le contenu de Pd était compris entre 0,5-2 % en poids et il a été utilisé un temps de photodéposition dans la gamme 15-20 minutes. Les poudres Pd-$TiO_2$ ont été caractérisées par diffraction des rayons X (XRD), surface spécifique BET ($S_{BET}$), fluorescence X (XRF), spectrométrie UV visible (UV vis DRS), microscopie

électronique à transmission (TEM) et spectrométrie photo électronique X (XPS). Il a été constaté que le chargement inférieur de Pd (0,5 % en poids) et 120 minutes de temps de photodéposition conduit à une répartition homogène des nanoparticules métalliques avec une faible dimension ; il a aussi été observé que l'augmentation de la charge de métal et celle de durée du dépôt conduisent à augmenter les espèces de $Pd^0$ efficacement déposées sur la surface de $TiO_2$. La taille des particules et l'état d'oxydation du palladium ont été les principaux facteurs qui influent sur l'activité photocatalytique et sur la sélectivité. La présence de palladium sur la surface de l'oxyde de titane accroit la production de $H_2$ et $CH_4$. En fait, sur le catalyseur avec 0,5 % en poids du chargement de Pd et 120 min de temps de photodéposition, il a été obtenu une production de $H_2$ d'environ 26 µmol après 3 heures de temps d'irradiation, quantité supérieure à celle obtenue avec $TiO_2$ sans Pd (environ 8,5 µmol). Le même résultat a été obtenu pour la production de méthane. Le pH initial de la solution a fortement influencé la sélectivité du système. Dans des conditions plus acides, la production de $H_2$ a été améliorée, tandis que la formation de $CH_4$ a été plus élevée pour des conditions alcalines.

## INTRODUCTION

In recent years, there have been intensive efforts toward the development of novel technologies for the production of hydrogen or methane from renewable resources, mainly water and biomass [1-3]. In particular, the food industry produces a large amount of solid and liquid wastes which could be valorized. In wastewater from the food industry, it is possible to find a high concentration of glucose. Glucose can be converted into hydrogen by several reactions, such as steam reforming [4, 5], wet oxidation of glucose [6], oxidative glucose reforming [7], pyrolysis [8], biophotolysis [9, 10], dark fermentation [11], electrolysis [12] and photocatalysis [13, 14]. Hydrogen has been identified as an ideal energy carrier for sustainable energy development [15-18] and it can be used in a fuel cell to generate electricity with high efficiency. In order to support a sustainable hydrogen economy, it is crucial to produce hydrogen cleanly and renewably. Typically, heterogeneous photocatalysis is studied with the aim of removing organic pollutants from wastewater [19, 20] through oxidation reactions which can finally result in the production of $CO_2$ and water. An interesting approach is to explore, in parallel to wastewater treatment, opportunities of mass recovery which can be sold as secondary raw material or used as energy resources, such as hydrogen and methane. Some wastewaters from food processes contain a high concentration of sugars, particularly glucose, which should be removed before effluent disposal or reuse, but if properly treated, hydrogen could be produced. In the past two decades, photocatalytic processes have been investigated as a possible method to obtain hydrogen glucose aqueous solutions [21]. The photocatalytic hydrogen production by decomposition of water containing glucose seems to have become a very powerful method for the practical and low-cost technologies in the hydrogen based energy system [22, 23]. Different catalysts containing noble metals on the surface (Au, Pt, Pd) or nanostructured $Fe_2O_3$ polymorphs [24] have been investigated [22, 25] because the presence of noble metals on the surface of the semiconductor improves photocatalytic performances. Linsebigler *et al.* (1995) [26] observed that by adding a small amount of noble metals, it is possible to suppress to some extent the charge recombination by forming a Schottky barrier. Rh or Pt, Pd, Cu or Ni supported on $TiO_2$ have been investigated in the conversion of glucose into $H_2$ [27]. However, the reactor configurations reported in the literature only include the use of mercury vapor lamps with high voltage as a light source (125-400 W) [28, 29]. Moreover, a few results are reported in the scientific literature about the production of methane through photocatalytic reforming of wastewater. Generally, the production of methane derives from processes such as anaerobic digestion [30, 31]. The production of hydrogen or methane from ethanol by photocatalytic reaction has also been reported [32].

In this work, the simultaneous production of $CH_4$ and $H_2$ from photocatalytic reforming of glucose on Pd-$TiO_2$ was investigated under UV light irradiation by Light-Emitting Diodes (LED) with low energy consumption (10 W). $TiO_2$ was prepared *via* a sol–gel technique, while Pd addition was carried out by photodeposition. The influence of some parameters, such as: photodeposition time and Pd loading on the final properties of the materials and their photocatalytic efficiency for glucose reforming was evaluated. The effect of the photocatalyst dosage and initial pH on photocatalytic performance was also investigated.

## 1 EXPERIMENTAL

### 1.1 Synthesis of Photocatalysts

$TiO_2$ was prepared by hydrolysis of titanium tetraisopropoxide (*Aldrich*, 97%) in isopropanol solution (1.6M) by the slow addition of distilled water (volume ratio

isopropanol/water 1:1). The $TiO_2$ powder was recovered by filtration, dried at 110°C for 24 h and pre-treated by immersion in a 1M sulfuric acid solution under continuous stirring for 1 h. After pre-treatment, the solution was filtered, dried and calcinated at 650°C for 2 h; the resulting photocatalyst was used as starting material (S-$TiO_2$). The fresh $TiO_2$ powder was submitted to a sulfate treatment, taking into account that previous results have shown that sulfate pre-treatment stabilizes the anatase phase up to high temperatures and protects the surface area against sintering [33-36].

Photodeposition of palladium was performed over the sulfated $TiO_2$ powders using palladium chloride (II) ($PdCl_2$, *Aldrich* 99%) as the metal precursor. Under an inert atmosphere ($N_2$), a suspension of the corresponding $TiO_2$ sample in distilled water containing isopropanol (*Merck* 99.8%), which acts as the sacrificial donor, was prepared. Then, the appropriate amount of $PdCl_2$ solution to obtain the desired nominal palladium loading was added; in order to dissolve the metal precursor, the pH of this solution was adjusted to 2 by using a HCl 0.1M solution. Photodeposition of palladium was then performed by illuminating the suspension for 120 min with an *Osram* Ultra-Vitalux lamp (300 W) which possesses a sun-like radiation spectrum with a main emission line in the UVA range at 365 nm. The light intensity on the suspensions was 60 W/m$^2$ determined by a PMA 2200 UVA photometer (*Solar Light Co.*). After photodeposition, the powders were recovered by filtration and dried at 110°C overnight. Series of Pd-$TiO_2$ catalysts were prepared by using different metal contents (0.5% or 2% weight total to $TiO_2$) and photodeposition times (15 or 120 min). The photocatalysts prepared by $TiO_2$ metallization will be denoted in this document as 0.5Pd15, 0.5Pd120, 2Pd15 and 2Pd120.

## 1.2 Photocatalyst Characterization

All the materials were widely characterized using different techniques. The crystalline phase composition and degree of crystallinity of the samples were estimated by XRD. XRD patterns were obtained on a *Siemens* D-501 diffractometer with a Ni filter and graphite monochromator using Cu Kα radiation. Anatase crystallite sizes were calculated from the line broadening of the main anatase XRD peak (101) by using the Scherrer equation. Peaks were fitted by using a Voigt function.

Specific surface area ($S_{BET}$) measurements were carried out using low-temperature nitrogen adsorption in a *Micromeritics ASAP* 2010 instrument. Degasification of the samples was performed at 150°C.

The chemical composition and total palladium content in the samples were determined by XRF in a *PANalytical Axios* sequential spectrophotometer equipped with a rhodium tube as the source of radiation. XRF measurements were performed on pressed pellets (sample included in 10 wt% of wax).

The light absorption properties of the samples were studied by UV-Vis spectroscopy. The UV-Vis DRS were recorded on a *Varian* spectrometer (model Cary 100) equipped with an integrating sphere and using $BaSO_4$ as a reference. Band-gap values were calculated from the corresponding Kubelka-Munk functions, F(R∞), which are proportional to the absorption of radiation by plotting $(F(R\infty)\cdot h\nu)^{1/2}$ against hν.

Palladium particle sizes were evaluated by TEM, in a *Philips* CM 200 microscope. The samples were dispersed in ethanol using an ultrasonicator and dropped on a carbon grid.

XPS studies were carried out on a *Leybold–Heraeus* LHS-10 spectrometer, working with a constant pass energy of 50 eV. The spectrometer's main chamber, working at a pressure $< 2 \times 10^{-9}$ Torr, is equipped with an EA-200 MCD hemispherical electron analyzer with a dual X-ray source working with Al Kα ($h\nu$ = 1 486.6 eV) at 120 wand 30 mA. The C 1s signal (284.6 eV) was used as an internal energy reference in all the experiments. Samples were outgassed in the prechamber of the instrument at 150°C up to a pressure $< 2 \times 10^{-8}$ Torr to remove chemisorbed water.

## 1.3 Photocatalytic Tests

Photocatalytic experiments were carried out with a *Pyrex* cylindrical reactor (ID = 2.5 cm) equipped with a $N_2$ distributor device ($Q$ = 0.122 NL/min). The continuous mixing of the glucose solution and the photocatalyst was carried out by external recirculation of water through the use of a peristaltic pump. A thermocouple was inserted inside the reactor to monitor the temperature during irradiation. The photoreactor was irradiated by a strip composed of 15 UV-LED (nominal power: 10 W) with wavelength emission in the range 375-380 nm. The LED strip was positioned around the external surface of the reactor so that the light source uniformly irradiated the reaction volume (light intensity: 1.5 W/m$^2$). Typically, 0.04 g of catalyst was suspended in an 80-mL aqueous solution containing 500 mg/L of glucose ($D^+$ Glucose VWR, *Sigma-Aldrich*). The suspension was left in dark conditions for 2 hours to reach the adsorption-desorption equilibrium of glucose on the photocatalysts' surface, and then a photocatalytic reaction was initiated under UV light for up to 3 hours. Hydrogen and methane yield during the irradiation time is evaluated according to the following relationship:

$$R_{H_2} = \frac{2 \cdot n_{H_2}}{12 \cdot n^0_{C_6H_{12}O_6}} \cdot 100$$

$$R_{CH_4} = \frac{4 \cdot n_{CH_4}}{12 \cdot n^0_{C_6H_{12}O_6}} \cdot 100$$

where: $R$ = yield; $n_{H_2}$ = moles of $H_2$ produced; $n_{CH_4}$ = moles of $CH_4$ produced; $n^0_{C_6H_{12}O_6}$ = moles of glucose after dark adsorption.

To evaluate the influence of the initial pH on the production of $H_2$ and $CH_4$, the pH of the solution was changed by adding nitric acid (*Baker* Analyzed, 65%) or ammonium hydroxide (*Baker* Analyzed, 30%). About 2 mL of samples were taken from the photoreactor at different times and filtered in order to remove Pd-$TiO_2$ particles before analysis.

### 1.4 Chemical Analysis

The analysis of the gaseous phase from the photoreactor was performed by online gas chromatography (*MicroGC*, *Agilent*) with a TDX-01 column for the analysis of CO, $CO_2$, $CH_4$ and $H_2$ and equipped with a molecular sieve for the analysis of oxygen. The concentration of glucose was measured by a spectrophotometric method [37, 38]. Briefly, a 2-mL aliquot of a carbohydrate solution is mixed with 1 mL of 5 wt% aqueous solution of phenol (*Sigma-Aldrich*) in a test tube. Subsequently, 5 mL of concentrated sulfuric acid (*Sigma-Aldrich*) is added rapidly to the mixture. Then, light absorption at 490 nm is recorded on a UV-Vis spectrophotometer (*Perkin Elmer*).

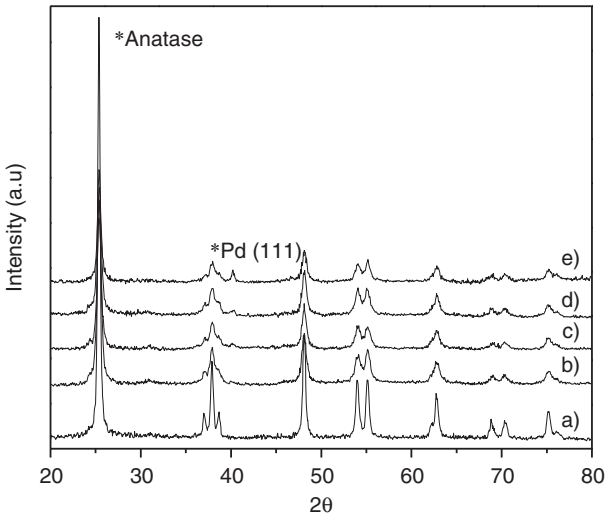


Figure 1

XRD patterns for $TiO_2$ and Pd-$TiO_2$ photocatalysts prepared with different Pd contents and deposition times. a) $TiO_2$; b) 0.5 wt% Pd-$TiO_2$, 15 min; c) 0.5 wt% Pd-$TiO_2$, 120 min; d) 2 wt% Pd-$TiO_2$, 15 min; e) 2 wt% Pd-$TiO_2$, 120 min.

## 2 RESULTS AND DISCUSSION

### 2.1 Photocatalyst Characterization

#### 2.1.1 X-Ray Diffraction

Figure 1 shows the XRD patterns of the Pd-$TiO_2$ photocatalysts; the only crystalline phase present in all the samples was anatase, identified by the main XRD peak located at 25.25°, thus indicating that the sulfation pre-treatment inhibited the formation of the rutile phase of $TiO_2$ during the calcination process, as has been reported by different authors [33-36].

On the other hand, photodeposition of palladium did not affect the phase composition in any case. In the spectra of metallized samples, a diffraction peak for Pd was detected at 40°; this peak is assigned to Pd (111) [39]. It was observed that the intensity of this peak increased with the Pd loading, being highest in the catalysts prepared with 2 wt% of nominal content and 120 min of deposition time; this could be due to a higher metal particle size in these samples.

The anatase crystallite sizes calculated by the Scherrer equation from the (101) peak of the XRD pattern are listed in Table 1. As can be seen, the $TiO_2$ presents a value of 20 nm; the Pd addition did not significantly modify crystallite sizes beyond this value.

#### 2.1.2 BET Surface Area

BET surface area values ($S_{BET}$) for all the samples are shown in Table 1. As can be seen, Pd addition did not induce significant modifications in the $S_{BET}$ of the analyzed materials, and the observed slight decreases are probably due to pore blocking by metal deposits on the $TiO_2$ surface.

TABLE 1

Characterization of the investigated photocatalysts

| Photocatalyst | Pd nominal loading (wt%) | Photodeposition time (min) | Real Pd content (wt%)* | Sulfate amount (wt%) | $S_{BET}$ ($m^2/g$) | Band gap (ev)** |
|---|---|---|---|---|---|---|
| S-$TiO_2$ | 0 | – | – | 0.30 | 58 | 3.2 |
| 0.5Pd15 | 0.5 | 15 | 0.18 | 0.28 | 46 | 3.2 |
| 0.5Pd120 | 0.5 | 120 | 0.20 | 0.27 | 48 | 3.2 |
| 2Pd15 | 2 | 15 | 0.34 | 0.28 | 48 | 3.2 |
| 2Pd120 | 2 | 120 | 0.80 | 0.28 | 49 | 3.2 |

### 2.1.3 X-Ray Fluorescence

The real palladium content in the metallized samples was measured by XRF and the values are listed in Table 1. These values are less than the nominal metal content used to prepare these materials (0.5 or 2 wt%), indicating an incomplete reduction of the metal precursor ($PdCl_2$) on the $TiO_2$ surface during the photodeposition process. However, the amount of deposited Pd was highest in the samples prepared with the highest deposition time (120 min).

In all the samples, XRF analysis revealed that a certain amount of S and $Cl^-$ species remained on the solid after preparation. The sulfur content was between 0.27 and 0.30%, and the chloride content was below 0.02%.

### 2.1.4 UV-Vis Diffuse Reflectance Spectra

The absorption spectra of all the samples are shown in Figure 2. The typical absorption band edge of the $TiO_2$ semiconductor was observed at around 400 nm for all the samples. As can be seen, metallization did not substantially alter the absorption properties of the samples; however, a slight increase in absorption throughout the visible range of the spectrum was observed due to the gray color of these materials; this increase is more evident in samples with the highest Pd loading.

From the UV-Vis DRS spectra, band-gap energies were calculated, being 3.20 eV for the $TiO_2$ corresponding to the anatase phase. Pd photodeposition did not induce any significant change in this value; estimated band-gap energies are between 3.2 and 3.3 eV.

### 2.1.5 Microscopic Analysis

The morphology and Pd particle size in the samples prepared was studied by TEM.

As was observed from the TEM images, in the samples prepared with 0.5 wt% Pd loading, metal nanoparticles appear to be homogenously distributed all over the surface, with sizes around 2-4 nm (images are not shown).

Figure 3 shows representative TEM images of $TiO_2$ after photodeposition of 2 wt% Pd with irradiation times of 15 and 120 min (Fig. 3a and 3b, respectively). In both samples, palladium particles can be seen as dark spherical spots placed on the larger anatase particles; in these samples Pd nanoparticles are heterogeneously distributed on the $TiO_2$ surface and particle sizes higher than 6 nm were observed.

### 2.1.6 XPS Analyses

XPS measurements were performed and a summary of these results is reported in Table 1.

Figure 4 shows spectra of Ti 2p and O 1s for the different samples analyzed. The Ti 2p core peaks exhibit a main component at around 458.5 ± 0.1 eV (Ti $2p_{3/2}$) in all the samples, representative of the $Ti^{4+}$ ions in the $TiO_2$ lattice. The addition of Pd did not modify the oxidation state or the chemical environment of titanium atoms at the surface of the $TiO_2$. In the O 1s region, a peak located at 529.8 ± 0.2 eV can be observed for all the samples, assigned to oxygen atoms in the $TiO_2$ lattice. This peak is asymmetric, with a shoulder at higher binding energies assigned to surface OH groups. The shoulder is more prominent in the non-metallized $TiO_2$ sample, indicating a higher hydroxylation degree in

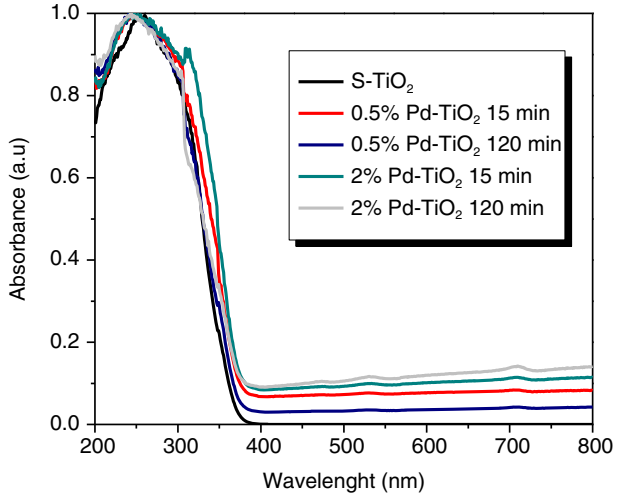


Figure 2

UV-Vis DRS spectra for the investigated photocatalysts.

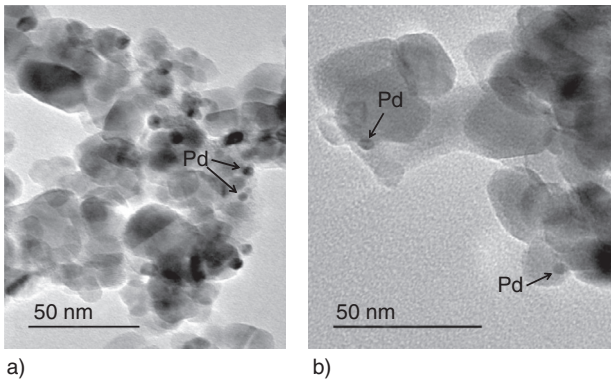


Figure 3

TEM images of 2 wt% Pd-$TiO_2$ samples. a) Pd-$TiO_2$, 15 min; b) Pd-$TiO_2$, 120 min.

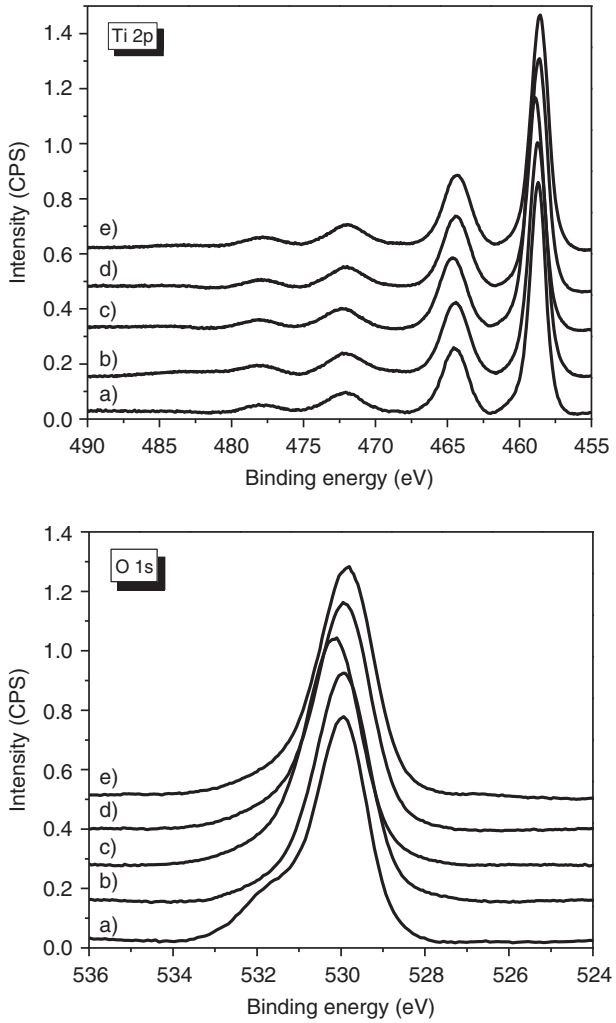


Figure 4

XPS core level spectra of Ti 2p and O 1s regions for the investigated photocatalysts. a) S-$TiO_2$; b) 0.5 wt% Pd-$TiO_2$, 15 min; c) 0.5 wt% Pd-$TiO_2$, 120 min; d) 2 wt% Pd-$TiO_2$, 15 min; e) 2 wt% Pd-$TiO_2$, 15 min.

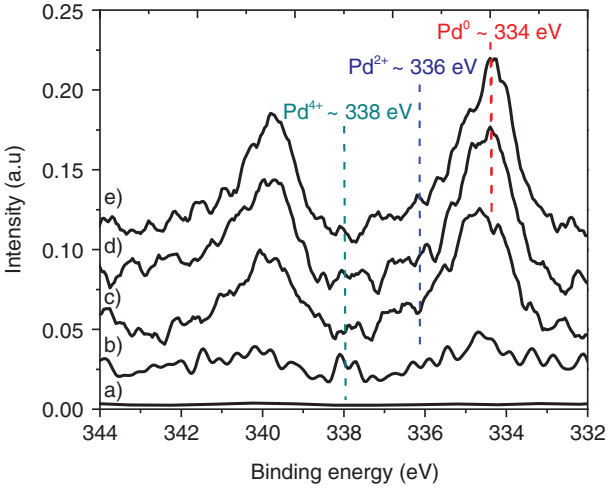


Figure 5

Comparative XPS spectra of Pd $3d_{7/2}$ and $3d_{7/2}$ core levels of Pd-$TiO_2$ catalysts prepared with different Pd contents and deposition times. a) S-$TiO_2$; b) 0.5 wt% Pd-$TiO_2$, 15 min; c) 0.5 wt% Pd-$TiO_2$, 120 min; d) 2 wt% Pd-$TiO_2$, 15 min; e) 2 wt% Pd-$TiO_2$, 120 min.

this sample. The intensity of this shoulder is lower in Pd-$TiO_2$ samples; this is mainly due to the presence of metallic nanoparticles partially covering the $TiO_2$ surface, as was observed by TEM (Fig. 3).

The study of XPS Pd 3d peak regions can provide information concerning the oxidation state of the Pd species adsorbed on the $TiO_2$ surface. A Pd 3d region is formed by a doublet corresponding to the signals for $3d_{7/2}$ and $3d_{5/2}$. The Pd $3d_{7/2}$ binding energy for metallic palladium ($Pd^0$) appears near to 334 eV, while for partially oxidized forms ($Pd^{2+}$/$Pd^{4+}$) it appears at higher binding energies with values of ca. 336 and 338 eV, respectively [40]. The XPS Pd 3d region for the Pd-$TiO_2$ samples prepared with 0.5 and 2 wt% metal content and deposition times of 15 and 120 min is shown in Figure 5. All the spectra were calibrated with the C 1s peak at 284.6 eV attributed to "adventitious" surface carbon. $Pd^0$ and $Pd^{\sigma+}$ species were detected in all the analyzed samples, thus indicating an incomplete reduction of the metal precursor on the $TiO_2$ surface; these observations are in agreement with the results obtained by XRF analysis (Sect. 2.1.3). However, the $Pd^0$ on $TiO_2$ increased with the deposition time and with the metal content. As can be seen qualitatively in Figure 5, the highest intensity of the peaks assigned to $Pd^0$ species content was observed in the catalyst prepared with 120 min of deposition time and 2 wt% of nominal Pd loading.

Pd $3d_{7/2}$ and $3d_{5/2}$ doublets were deconvoluted using the UNIFIT 2009 software assuming a doublet separation of 5.2 eV of the two components. The spectrum obtained for the 2 wt% Pd-$TiO_2$ catalysts prepared with 120 min of deposition time is shown in Figure 6. A Shirley-type background was subtracted from each spectrum. By the deconvolution of the doublets, it is possible to observe clearly the presence of $Pd^0$/$Pd^{\sigma+}$ species in the analyzed sample.

## 2.2 Photocatalytic Results

### 2.2.1 Influence of Photocatalyst Formulation

The preliminary test performed in dark conditions showed no reaction product in the gaseous phase.

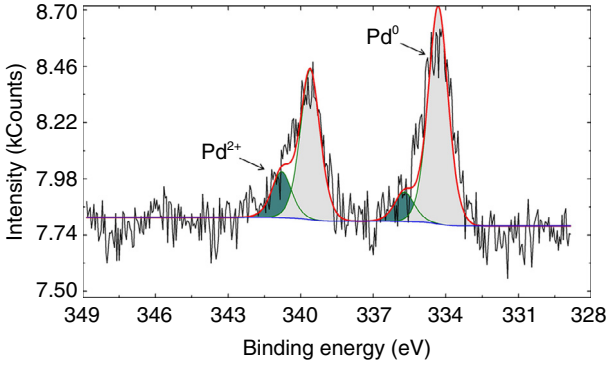


Figure 6

XPS Pd $3d_{7/2}$ and $3d_{7/2}$ regions for the 2 wt% Pd-$TiO_2$ catalyst prepared with 120 min of deposition time.

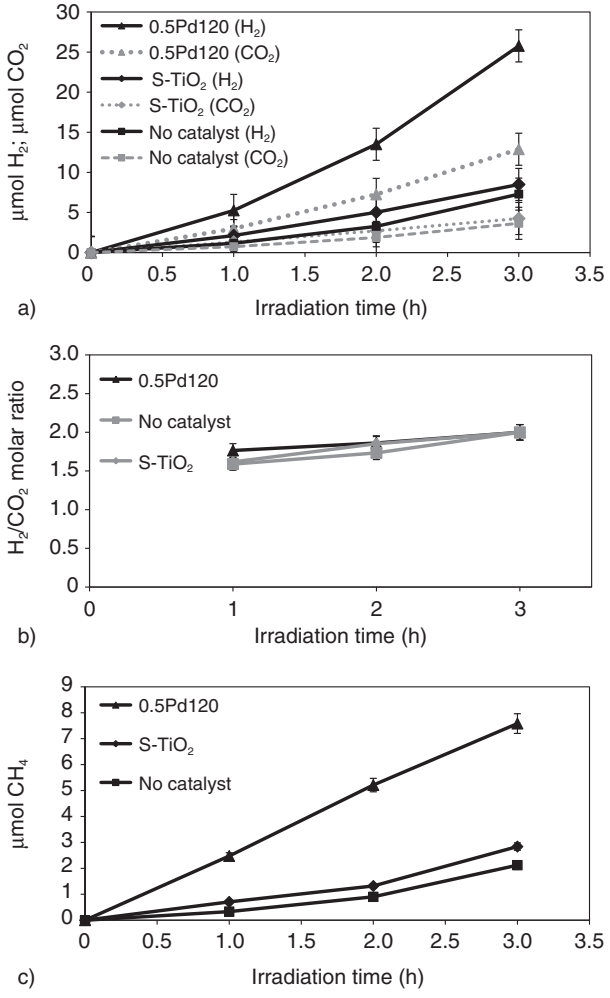


Figure 7

Control tests with UV as a standalone process and under photocatalytic conditions with UV/S-$TiO_2$ and UV/0.5Pd120: $H_2$ and $CH_4$ production a), $H_2/CO_2$ molar ratio b) and $CH_4$ production c).

The final concentration of glucose after the dark period was 351 and 305 mg/L for S-$TiO_2$ and 0.5Pd120, respectively.

Control tests with UV as a standalone process and under photocatalytic conditions with UV/S-$TiO_2$ and UV/0.5Pd120 were carried out to evaluate the contribution of each process in the production of hydrogen and methane from glucose (Fig. 7). During the irradiation time, the production of $H_2$, $CO_2$ and $CH_4$ was observed, but no formation of CO and $O_2$ was observed. The presence of palladium photodeposited on the surface of the titania enhanced the production of hydrogen (Fig. 7a). In particular, a production of $H_2$ as high as 26 μmol ($R_{H_2}$= 3%) after 3 hours of irradiation with a 0.5Pd120 catalyst was observed. The hydrogen yield on 0.5Pd120 (3%) is significantly higher than that obtained on S-$TiO_2$ (0.9%). However, a large fraction of glucose is not converted into hydrogen and methane under the present conditions.

These results are in agreement with those reported in the literature. In particular, loading noble metals such as Pt [41] and Au [42] onto the photocatalyst surface can separate photogenerated electrons and holes more effectively and thus improve hydrogen production. In a similar way, the coexistence of Pd with $TiO_2$ in the Pd-$TiO_2$ composite photocatalyst may lower the recombination rate between photogenerated electrons and holes, thus improving the efficiency of the photocatalysis process. It is well known that there are two forms of electron-hole recombination in $TiO_2$, surface recombination and bulk recombination, and both can lower the efficiency of photocatalysis [43]. The Fermi energy level of Pd is lower than that of $TiO_2$, and since they are closer to each other, the electrons on the surface of $TiO_2$ can spontaneously transfer to the surface of Pd until their Fermi energy levels become equal. As a result, excessive negative charges accumulate on the surface of Pd and excessive positive charges accumulate on the surface of $TiO_2$. Therefore, the energy band of $TiO_2$ bends upwards, forming the Schottky barrier. Therefore, in the composite catalyst, Pd acts as an electron trap, which can effectively prevent the surface electron-hole recombination [43].

The value of the $H_2/CO_2$ molar ratio did not change significantly as irradiation time increased, tending to a value approximately equal to 2 after three hours of irradiation (Fig. 7b). $CO_2$ and $H_2$ are mainly produced from the photocatalytic wet reforming of glucose, according to the following reaction (Eq. 1):

$$C_6H_{12}O_6(l) + 6\ H_2O(l) = 6\ CO_2(g) + 12\ H_2(g) \quad (1)$$

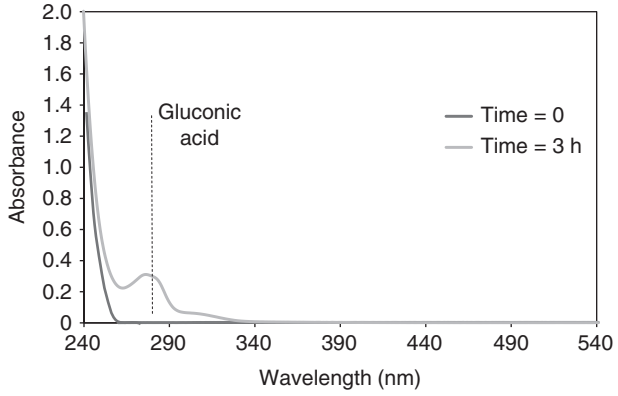


Figure 8

Spectrophotometric analysis of the aqueous solution before and after treatment with the 0.5Pd120 catalyst.

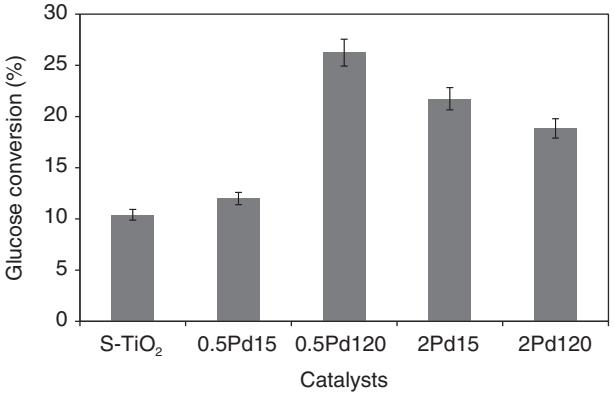


Figure 9

Glucose conversion after photocatalytic treatment by S-$TiO_2$ and Pd-$TiO_2$ catalysts (3 h irradiation time).

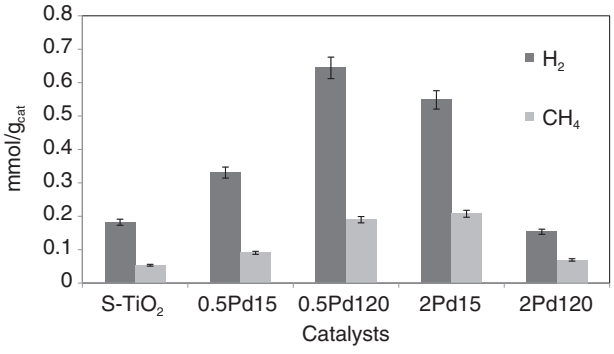


Figure 10

$H_2$ and $CH_4$ production after photocatalytic treatment by S-$TiO_2$ and Pd-$TiO_2$ catalysts (3 h irradiation time).

The deposition of Pd (0.5Pd120) resulted in an increased methane production (7.58 µmol) and yield (2%) compared with the S-$TiO_2$ catalyst, for which $CH_4$ production and yield were about 2.8 µmol and 0.6%, respectively (Fig. 7c).

In the absence of oxygen, methane could result from the degradation of glucose through the following reaction (Eq. 2) [44]:

$$C_6H_{12}O_6(l) = 3\ CH_4(g) + 3\ CO_2(g) \qquad (2)$$

Since $CO_2$ mainly comes from the photocatalytic wet reforming of glucose (Eq. 1), as confirmed by the molar ratio $H_2/CO_2$ being equal to 2, $CH_4$ could be formed through the following reaction (Eq. 3), similar to anaerobic digestion:

$$C_6H_{12}O_6(l) + 6\ H_2O(l) = 6\ CH_4(g) + 6\ O_2(g) \qquad (3)$$

This result is confirmed by the analysis of the liquid phase after 3 hours of irradiation, which showed the presence of gluconic acid (Fig. 8), a typical product of glucose oxidation [45]. Therefore, the oxygen produced according to Equation (3) possibly reacts with glucose, leading to the formation of gluconic acid. The presence of the latter was detected by spectrophotometric analysis of the liquid sample whose result is reported in Figure 8; gluconic acid is represented by a band with a peak at a wavelength of 254 nm [45]. The presence of any intermediate compounds that have been produced by the oxidation of glucose, such as gluconic acid, is important because they may possibly be recovered and used for different purposes (food, pharmaceutical and hygienic products) [45].

Glucose conversions observed during S-$TiO_2$ and Pd-$TiO_2$ photocatalytic treatment after 3 hours of irradiation are shown in Figure 9. The photocatalytic activity of Pd-$TiO_2$ was influenced by the photodeposition time and by the content of palladium used in the synthesis of the photocatalysts. The increase in the photodeposition time up to 120 min had a positive effect on the $TiO_2$ photoactivity for 0.5 wt% of Pd loading. Glucose conversion values obtained with the catalysts with 2 wt% of Pd content were lower than those obtained with the catalysts with 0.5 wt% of Pd loading, for both deposition times investigated. In particular, the best catalyst for the conversion of glucose was 0.5Pd120, for which the glucose conversion was as high as 26%.

This result is in agreement with the production of hydrogen and methane (Fig. 10); the highest production of $H_2$ and $CH_4$ was observed for the catalyst 0.5Pd120. In particular, on this catalyst it is possible to obtain 0.65 mmol/$g_{cat}$ of $H_2$ and 0.18 mmol/$g_{cat}$ of $CH_4$.

It is very important to note that the hydrogen production is very similar to that obtained by using a UV lamp with a nominal power of 125 W [29].

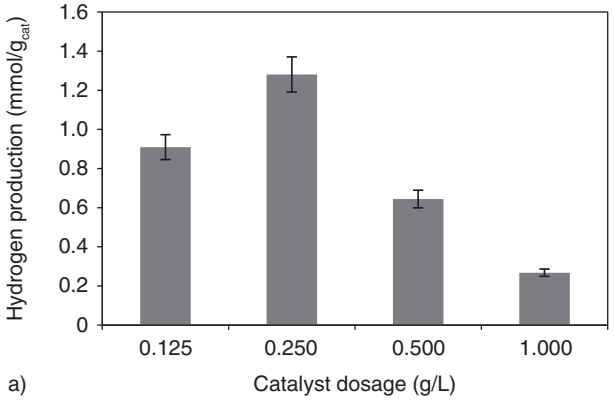


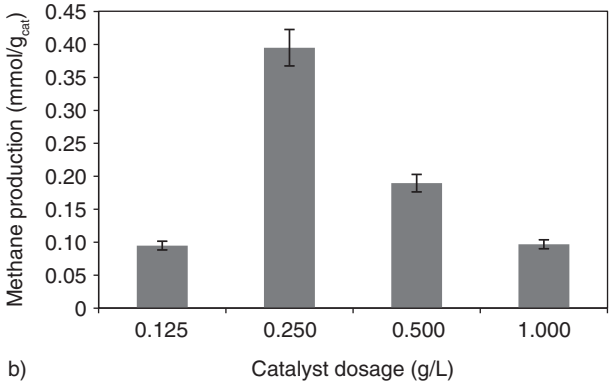


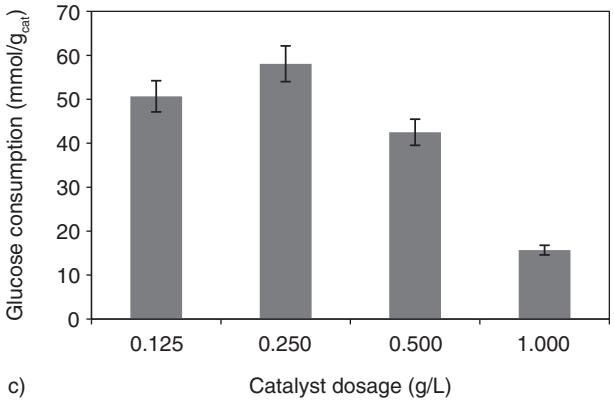


Figure 11

Optimization of catalyst loading according to hydrogen a) and methane b) production, and glucose consumption c).

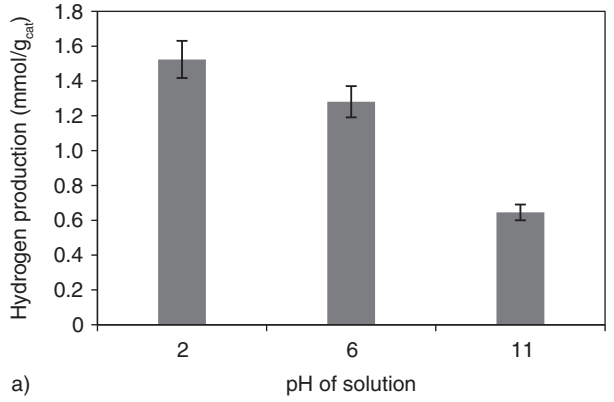


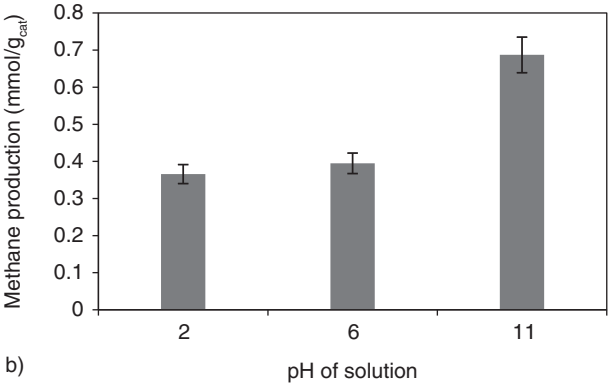


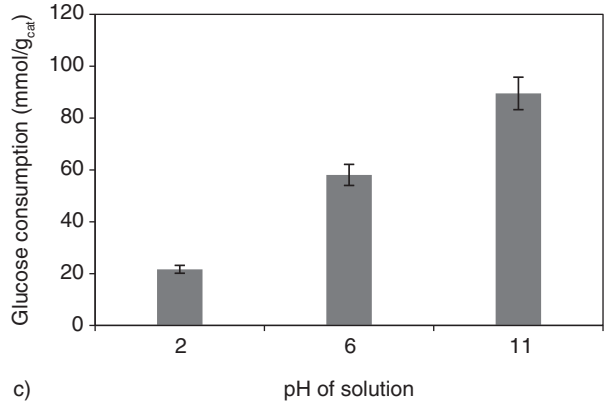


Figure 12

Effect of the initial pH on hydrogen a) and methane b) production, and glucose consumption c).

The behavior observed could be explained taking into account that in the analyzed photocatalysts partially oxidized Pd species and metallic Pd were detected. These species could be responsible for the differences observed in the glucose conversion and hydrogen production in the glucose reforming over Pd-$TiO_2$ photocatalysts. The catalyst prepared with 0.5 wt% Pd loading and 120 min of photodeposition time resulted in the highest glucose conversion and $H_2$ production. The highest performances are possibly related to a homogeneous Pd nanoparticle distribution over the $TiO_2$ surface with sizes lower than 4 nm (as observed by TEM analysis) and $Pd^0$ oxidation state (according to XPS analysis, metal preferentially occurs in its metallic state ($Pd^0$)).

For the catalysts with a Pd content higher than 0.5 wt%, the presence of $Pd^{\delta+}$ species on the $TiO_2$ surface could induce a preferential Pd photodeposition on these species,

not over $TiO_2$, leading to an increase in the Pd particle size. Moreover, the metal oxidation state can modify the adsorption of glucose on the photocatalyst surface, thus determining a different catalytic activity.

### 2.2.2 Optimization of Catalyst Dosage for Photocatalytic Tests

The optimization of the catalyst dosage was carried out under UV irradiation by testing different concentrations of 0.5Pd120 photocatalysts, in the range 0.125-1 g/L. Photocatalytic efficiency increased as catalyst loading was increased up to 0.25 g/L. As catalyst loading was further increased, the conversion of glucose and the simultaneous formation of $H_2$ and $CH_4$ decreased (Fig. 11).

Possibly, the increase in the catalyst dosage over the optimum value resulted in a decreased light penetration through the solution because of the increased opacity of the aqueous suspension [46].

### 2.2.3 Influence of Initial pH of Solution

Finally, the effect of the pH on the production of hydrogen (Fig. 12a) and methane (Fig.12b) as well as on the conversion of glucose (Fig. 12c) was evaluated. The specific conversion of glucose increased as the solution pH was increased. The effects of pH on hydrogen generation are considered to be quite complex, involving the changes of the chemical state of glucose, redox potential of $H^+/H_2$ and relative position of the band edges of the semiconductor [47]. At lower pH values (pH = 3), the redox potential of $H^+/H_2$ would become more positive, which is advantageous for efficient hydrogen generation [47]. However, the most favorable condition for methane production is alkaline solution. Accordingly, the highest methane production was observed at pH 11 (about twice that at pH 3). Possibly, when the redox potential of $H^+/H_2$ becomes more negative and the pH of the solution is similar to the $pk_a$ of glucose, the methane production is enhanced.

## CONCLUSIONS

Pd deposition onto the sulfated $TiO_2$ surface throughout the photodeposition time was favorable to the production of $H_2$ or $CH_4$ by photocatalysis. These compounds were produced efficiently by photocatalytic reforming of aqueous solutions of glucose. The experimental conditions during photodeposition, such as deposition time, were found to have a strong influence on the final properties of the materials, and consequently on their photocatalytic activity in glucose reforming. A short deposition time (15 min) led to a smaller average particle size and higher dispersion of the palladium on the sulfated $TiO_2$ surface, as well as a higher fraction of the metal in its metallic state. These features resulted in a good photocatalytic performance in terms of glucose conversion. The best photocatalytic behavior was observed in the sample prepared with 0.5 wt% of palladium and 120 min of photodeposition time. By changing the pH of the solution, it is possible to modulate the performance of the photocatalytic reaction, producing more methane in alkaline conditions or more hydrogen in acidic conditions.

The process appears to be a promising, cost-effective method (also considering the high energy-efficiency lighting by UVA-LED) for the treatment of sugar water from industrial food processes, with a parallel recovery of products ($CH_4$ and $H_2$) which could be successfully used for energy production.

## ACKNOWLEDGMENTS

J.J. Murcia would like to thank the CSIC for the concession of a JAE grant. CITIUS (University of Seville) is acknowledged for XPS and XRF measurements.
Diana Sannino wishes to thank the University of Salerno for funding the project "ORSA111873; *Processi chimici catalitici per la produzione di energia sostenibile e l'ambiente*".

## REFERENCES

1 Turner J.A. (2004) Sustainable Hydrogen Production, *Science* **305**, 5686, 972-974.

2 Fu X., Long J., Wang X., Leung D.Y.C., Ding Z., Wu L., Zhang Z., Li Z., Fu X. (2008) Photocatalytic reforming of biomass: A systematic study of hydrogen evolution from glucose solution, *International Journal of Hydrogen Energy* **33**, 22, 6484-6491.

3 Kondarides D.I., Patsoura A., Verykios X.E. (2010) Anaerobic Photocatalytic Oxidation of Carbohydrates in Aqueous $Pt/TiO_2$ Suspensions with Simultaneous Production of Hydrogen, *J. Adv. Oxid. Technol.* **13**, 1, 116-123.

4 Azadi P., Otomo J., Hatano H., Oshima Y., Farnood R. (2010) Hydrogen production by catalytic near-critical water gasification and steam reforming of glucose, *International Journal of Hydrogen Energy* **35**, 8, 3406-3414.

5 Bičáková O., Straka P. (2012) Production of hydrogen from renewable resources and its effectiveness, *International Journal of Hydrogen Energy* **37**, 16, 11563-11578.

6 Moreno T., Kouzaki G., Sasaki M., Goto M., Cocero M.J. (2012) Uncatalysed wet oxidation of d-glucose with hydrogen peroxide and its combination with hydrothermal electrolysis, *Carbohydrate Research* **349**, 33-38.

7 Prüße U., Herrmann M., Baatz C., Decker N. (2011) Gold-catalyzed selective glucose oxidation at high glucose concentrations and oxygen partial pressures, *Applied Catalysis A: General* **406**, 1-2, 89-93.

8 Foster A.J., Jae J., Cheng Y.-T., Huber G.W., Lobo R.F. (2012) Optimizing the aromatic yield and distribution from catalytic fast pyrolysis of biomass over ZSM-5, *Applied Catalysis A: General* **423-424**, 154-161.

9 Hallenbeck P.C., Abo-Hashesh M., Ghosh D. (2012) Strategies for improving biological hydrogen production, *Bioresource Technology* **110**, 1-9.

10 Ntaikou I., Gavala H.N., Kornaros M., Lyberatos G. (2008) Hydrogen production from sugars and sweet sorghum biomass using Ruminococcus albus, *International Journal of Hydrogen Energy* **33**, 4, 1153-1163.

11 Lee H.S., Salerno M.B., Rittmann B.E. (2008) Thermodynamic evaluation on $H_2$ production in glucose fermentation, *Environmental Science & Technology* **42**, 7, 2401-2407.

12 McGinley J., McHale F.N., Hughes P., Reid C.N., McHale A.P. (2004) Production of electrical energy from carbohydrates using a transition metal-catalysed liquid alkaline fuel cell, *Biotechnology Letters* **26**, 23, 1771-1776.

13 Kawai T., Sakata T. (1980) Conversion of carbohydrate into hydrogen fuel by a photocatalytic process, *Nature* **286**, 5772, 474-476.

14 Bahruji H., Bowker M., Davies P.R., Al-Mazroai L.S., Dickinson A., Greaves J., James D., Millard L., Pedrono F. (2010) Sustainable $H_2$ gas production by photocatalysis, *Journal of Photochemistry and Photobiology A: Chemistry* **216**, 2-3, 115-118.

15 Song C. (2002) Fuel processing for low-temperature and high-temperature fuel cells: Challenges, and opportunities for sustainable development in the 21st century, *Catal. Today* **77**, 1-2, 17-49.

16 Hamelinck C.N., Faaij A.P.C. (2002) Future prospects for production of methanol and hydrogen from biomass, *Journal of Power Sources* **111**, 1, 1-22.

17 Bridgwater A.V. (1994) Catalysis in thermal biomass conversion, *Applied Catalysis A: General* **116**, 1-2, 5-47.

18 Huber G.W., Shabaker J.W., Dumesic J.A. (2003) Raney Ni-Sn catalyst for $H_2$ production from biomass-derived hydrocarbons, *Science* **300**, 5628, 2075-2077.

19 Vaiano V., Sacco O., Sannino D., Ciambelli P., Longo S., Venditto V., Guerra G. (2014) N-doped $TiO_2$/s-PS aerogels for photocatalytic degradation of organic dyes in wastewater under visible light irradiation, *J. Chem. Technol. Biotechnol.* **89**, 8, 1175-1181.

20 Vaiano V., Sacco O., Stoller M., Chianese A., Ciambelli P., Sannino D. (2014) Influence of the photoreactor configuration and of different light sources in the photocatalytic treatment of highly polluted wastewater, *Int. J. Chem. React. Eng.* **12**, 1, 1-13.

21 Mohamed R.M., Aazam E.S. (2012) $H_2$ Production with Low CO Selectivity from Photocatalytic Reforming of Glucose on Ni/$TiO_2$-$SiO_2$, *Chinese Journal of Catalysis* **33**, 2-3, 247-253.

22 Gomathisankar P., Yamamoto D., Katsumata H., Suzuki T., Kaneco S. (2013) Photocatalytic hydrogen production with aid of simultaneous metal deposition using titanium dioxide from aqueous glucose solution, *International Journal of Hydrogen Energy* **38**, 14, 5517-5524.

23 Zhang L., Shi J., Liu M., Jing D., Guo L. (2014) Photocatalytic reforming of glucose under visible light over morphology controlled $Cu_2O$: Efficient charge separation by crystal facet engineering, *Chemical Communications* **50**, 2, 192-194.

24 Carraro G., Maccato C., Gasparotto A., Montini T., Turner S., Lebedev O.I., Gombac V., Adami G., Van Tendeloo G., Barreca D., Fornasiero P. (2014) Enhanced Hydrogen Production by Photoreforming of Renewable Oxygenates Through Nanostructured $Fe_2O_3$ Polymorphs, *Advanced Functional Materials* **24**, 3, 372-378.

25 Kondarides D., Daskalaki V., Patsoura A., Verykios X. (2008) Hydrogen Production by Photo-Induced Reforming of Biomass Components and Derivatives at Ambient Conditions, *Catal Lett*. **122**, 1-2, 26-32.

26 Linsebigler A.L., Lu G., Yates J.T. (1995) Photocatalysis on $TiO_2$ Surfaces: Principles, Mechanisms, and Selected Results, *Chemical Reviews* **95**, 3, 735-758.

27 Chong R., Li J., Ma Y., Zhang B., Han H., Li C. (2014) Selective conversion of aqueous glucose to value-added sugar aldose on $TiO_2$-based photocatalysts, *Journal of Catalysis* **314**, 101-108.

28 Wu G., Chen T., Zhou G., Zong X., Li C. (2008) $H_2$ production with low CO selectivity from photocatalytic reforming of glucose on metal/$TiO_2$ catalysts, *Sci. China Ser. B-Chem.* **51**, 2, 97-100.

29 Colmenares J.C., Magdziarz A., Aramendia M.A., Marinas A., Marinas J.M., Urbano F.J., Navio J.A. (2011) Influence of the strong metal support interaction effect (SMSI) of Pt/$TiO_2$ and Pd/$TiO_2$ systems in the photocatalytic biohydrogen production from glucose solution, *Catalysis Communications* **16**, 1, 1-6.

30 Passio L., Rizzoa L., Fuchs S. (2012) Two-phase anaerobic digestion of partially acidified sewage sludge: a pilot plant study for safe sludge disposal in developing countries, *Environmental technology* **33**, 16-18, 2089-2095.

31 Li Y., Park S.Y., Zhu J. (2011) Solid-state anaerobic digestion for methane production from organic waste, *Renewable and Sustainable Energy Reviews* **15**, 1, 821-826.

32 Sakata T., Kawai T. (1981) Heterogeneous photocatalytic production of hydrogen and methane from ethanol and water, *Chemical Physics Letters* **80**, 2, 341-344.

33 Colón G., Hidalgo M.C., Navío J.A. (2003) Photocatalytic behaviour of sulphated $TiO_2$ for phenol degradation, *Applied Catalysis B* **45**, 1, 39-50.

34 Maicu M., Hidalgo M.C., Colón G., Navío J.A. (2011) Comparative study of the photodeposition of Pt, Au and Pd on pre-sulphated $TiO_2$ for the photocatalytic decomposition of phenol, *Journal of Photochemistry and Photobiology A: Chemistry* **217**, 2-3, 275-283.

35 Hidalgo M.C., Murcia J.J., Navío J.A., Colón G. (2011) Photodeposition of gold on titanium dioxide for photocatalytic phenol oxidation, *Applied Catalysis A: General* **397**, 1-2, 112-120.

36 Murcia J.J., Hidalgo M.C., Navío J.A., Araña J., Doña-Rodríguez J.M. (2014) Correlation study between photodegradation and surface adsorption properties of phenol and methyl orange on $TiO_2$ Vs platinum-supported $TiO_2$, *Applied Catalysis B* **150-151**, 107-115.

37 DuBois M., Gilles K.A., Hamilton J.K., Rebers P.A., Smith F. (1956) Colorimetric Method for Determination of Sugars and Related Substances, *Analytical Chemistry* **28**, 3, 350-356.

38 Albalasmeh A.A., Berhe A.A., Ghezzehei T.A. (2013) A new method for rapid determination of carbohydrate and total carbon concentrations using UV spectrophotometry, *Carbohydrate Polymers* **97**, 2, 253-261.

39 Navaladian S., Viswanathan B., Varadarajan T.K., Viswanath R.P. (2008) A Rapid Synthesis of Oriented Palladium Nanoparticles by UV Irradiation, *Nanoscale Research Letters* **4**, 2, 181-186.

40 Brun M., Berthet A., Bertolini J.C. (1999) XPS, AES and Auger parameter of Pd and PdO, *Journal of Electron Spectroscopy and Related Phenomena* **104**, 1-3, 55-60.

41 Siemon U., Bahnemann D., Testa J.J., Rodríguez D.Litter M.I. Bruno N. (2002) Heterogeneous photocatalytic reactions comparing $TiO_2$ and Pt/$TiO_2$, *Journal of Photochemistry and Photobiology A: Chemistry* **148**, 1-3, 247-255.

42 Bamwenda G.R., Tsubota S., Nakamura T., Haruta M. (1995) Photoassisted hydrogen production from a water ethanol solution a comparison of activities of Au-$TiO_2$ and Pt-$TiO_2$, *Journal of Photochemistry and Photobiology A: Chemistry* **89**, 2, 177-189.

43 Liu Y., Guo L., Yan W., Liu H. (2006) A composite visible-light photocatalyst for hydrogen production, *Journal of Power Sources* **159**, 2, 1300-1304.

44 Kenney J.F., Kutcherov V.A., Bendeliani N.A., Alekseev V.A. (2002) The evolution of multicomponent systems at high pressures: VI. The thermodynamic stability of the hydrogen–carbon system: The genesis of hydrocarbons and the origin of petroleum, *Proceedings of the National Academy of Sciences* **99**, 17, 10976-10981.

45 Ramachandran S., Fontanille P., Pandey A., Larroche C. (2006) Gluconic acid: Properties, applications and microbial production, *Food Technology and Biotechnology* **44**, 2, 185-195.

46 Sannino D., Vaiano V., Sacco O., Ciambelli P. (2013) Mathematical modelling of photocatalytic degradation of methylene blue under visible light irradiation, *Journal of Environmental Chemical Engineering* **1**, 1-2, 56-60.

47 Jing D., Liu M., Shi J., Tang W., Guo L. (2010) Hydrogen production under visible light by photocatalytic reforming of glucose over an oxide solid solution photocatalyst, *Catalysis Communications* **12**, 4, 264-267.

*Manuscript submitted in October 2014*
*Manuscript accepted in December 2014*
*Published online in March 2015*

**Cite this article as:** V. Vaiano, G. Iervolino, G. Sarno, D. Sannino, L. Rizzo, J.J.M. Mesa, M.C. Hidalgo and J.A. Navío (2015). Simultaneous Production of $CH_4$ and $H_2$ from Photocatalytic Reforming of Glucose Aqueous Solution on Sulfated Pd-$TiO_2$ Catalysts, *Oil Gas Sci. Technol* **70**, 5, 891-902.